Experimental and theoretical analyses of package-on-package structure under three-point bending loading*

Jia Su(贾 苏)[a], Wang Xi-Shu(王习术)[a]†, and Ren Huai-Hui(任淮辉)[a,b]

[a] *Department of Engineering Mechanics, AML, Tsinghua University, Beijing* 100084, *China*

[b] *China Longyuan Power Group Corporation Limited, China Goudian, Beijing* 100034, *China*

(Received 10 May 2012; revised manuscript received 23 July 2012)

High density packaging is developing toward miniaturization and integration, which causes many difficulties in designing, manufacturing, and reliability testing. Package-on-Package (PoP) is a promising three-dimensional high-density packaging method that integrates a chip scale package (CSP) in the top package and a fine-pitch ball grid array (FBGA) in the bottom package. In this paper, *in-situ* scanning electron microscopy (SEM) observation is carried out to detect the deformation and damage of the PoP structure under three-point bending loading. The results indicate that the cracks occur in the die of the top package, then cause the crack deflection and bridging in the die attaching layer. Furthermore, the mechanical principles are used to analyse the cracking process of the PoP structure based on the multi-layer laminating hypothesis and the theoretical analysis results are found to be in good agreement with the experimental results.

Keywords: high density package, *in-situ* SEM observation, three-point bending, multi-layer laminating hypothesis

PACS: 62.20.M–, 85.85.+j, 46.50.+a, 46.70.–p **DOI:** 10.1088/1674-1056/21/12/126201

1. Introduction

Owing to the increasing demands of electronic products with compact size, high functions, and high density mounting, packaging technologies of the ultra-large-scale integrated circuit (ULSIC) such as the quad flat package (QFP), ball grid array (BGA), chip scale package (CSP), and package-on-package (PoP) have rapidly developed in the past decades.[1−5] The high density package is marching toward miniaturization and integration, which augments difficulty in designing, manufacturing, reliable testing, and life prediction.[6] Package-on-package (PoP) is a promising three-dimensional (3D) high-density packaging method that integrates a chip scale package (CSP) in the top package and fine-pitch ball grid array (FBGA) in the bottom package.[7,8] It has been widely used in small communication terminals including cell phones, personal digital assistants, system boards, and so on.[2,9,10] A major advantage of PoP packaging is that the top and bottom package can be designed and tested individually before they are assembled, which makes the method widely used nowadays.[11]

Previous research indicated that cracking and delamination are the two main damage modes.[2,11−13] The ordinary testing methods on the reliability of stacked packages were used by detecting the electric resistance of the integrated circuit in order to verify whether the circuit board can work well.[14,15] These methods cannot directly detect the failure mechanism, crack developing process, and influencing factors of the device or element for the electronic packaging. Recently, simulation and experimental methods were used to investigate the failure modes of high-density package structures under mechanical and thermal loading, and lots of valuable findings have been achieved.[11,16] In the present paper, the processes of crack initiation and propagation under applied loading are observed based on the *in-situ* SEM technology, which can help to understand in depth the failure mechanism and crack initiation behaviour of stacked packages.[12,17−19] Furthermore, the different failure

*Projects supported by the National Natural Science Foundation of China (Grant Nos. 11072124 and 11272173), the National Basic Research Program of China (Grant No. 2010CB631006), and the State Key Laboratory of Advanced Metals and Materials, China (Grant No. 2010ZD-04).

†Corresponding author. E-mail: xshwang@tsinghua.edu.cn

© 2012 Chinese Physical Society and IOP Publishing Ltd

mechanisms assist us in optimizing the design and improving the reliability of stacked packages.

2. Experimental method and results

The novel PoP structure and its cross-sectional structure used in the failure tests are shown in Fig. 1. In Fig. 1(b), the multi-layer microstructure is clearly seen on the micro scale. Also, the experimental process is shown by using *in-situ* scanning electron microscopy (SEM) observation technology in order to obtain the micro failure mode of the structure.[18,20−22] The PoP structure consists mainly of the following parts:[23]

(i) a top package for the memory unit in stack chip scale package format with three dies equidistantly implanted into the plastic resin and a thick substrate in the bottom; a bottom package for logic operation in over-molded FBGA format with a die embedded into the plastic resin and a thick substrate;

(ii) the conductive leads and wiring bonding (WB) embedded in the plastic resin for interconnection purposes.

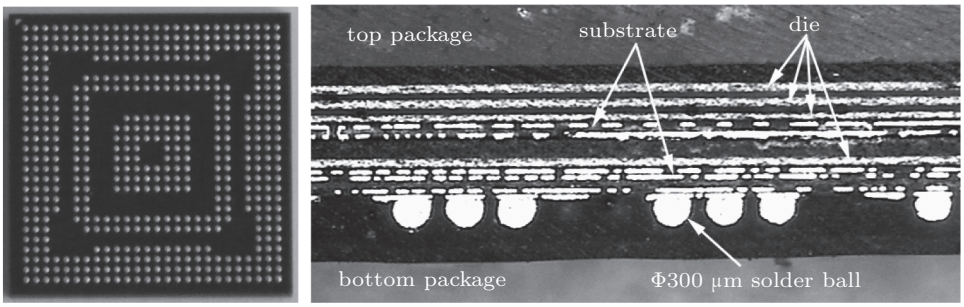


Fig. 1. Images of the PoP structure (where the bright spots are the solder balls) (a) and its cutting surface (b).

The size of the top package is 14 mm×14 mm× 0.7 mm (length × width × thickness). It is composed of a substrate and three dies (named die A, die B, die C from top to bottom in sequence), among which are the die attaches (DAs). All the above multi-layers are pasted by packaging adhesives and the dies are enclosed by the mold cap on the top of the substrate. The top package is connected with the bottom package by two rows of solder balls each with a diameter of about 500 μm. The size of the bottom package is 14 mm×14 mm×0.25 mm (length × width × thickness). Minor-sized solder balls are placed in the lower surface, and their diameters are all about 300 μm. The key parameters of both top and bottom packages are listed in Table 1.

Two kinds of three-point bending tests are conducted: one is the half-structure test in which the structure is cut into two identical parts according to the symmetry axis and the half part was used as the specimen; the other one is the one-quarter-structure test in which the boundary away from the symmetry of the half-structure is ground off. The two kinds of specimen are shown in Fig. 2. The cutting surfaces of the specimen is polished by abrasive paper P1000 and P2000 to investigate the crack initiation, and the crack propagation behaviour clearly.

Table 1. Key parameters of the top and bottom packages.

	Top package	Bottom package
Die size/mm	8×8×0.08 (die A, die B) 7.8×7.8×0.05 (die C)	7.6×7.6×0.08
Number of die	3	1
Mold body size/mm	14×14×0.6	10.8×10.8×0.35
Substrate size/mm	14×14×0.1275	14×14×0.1
Die attach material	die attach film	die attach film
Ball diameter/mm	0.5	0.3
Alloy of ball material	SnAgAu	SnAgAu
Number of ball	152	491

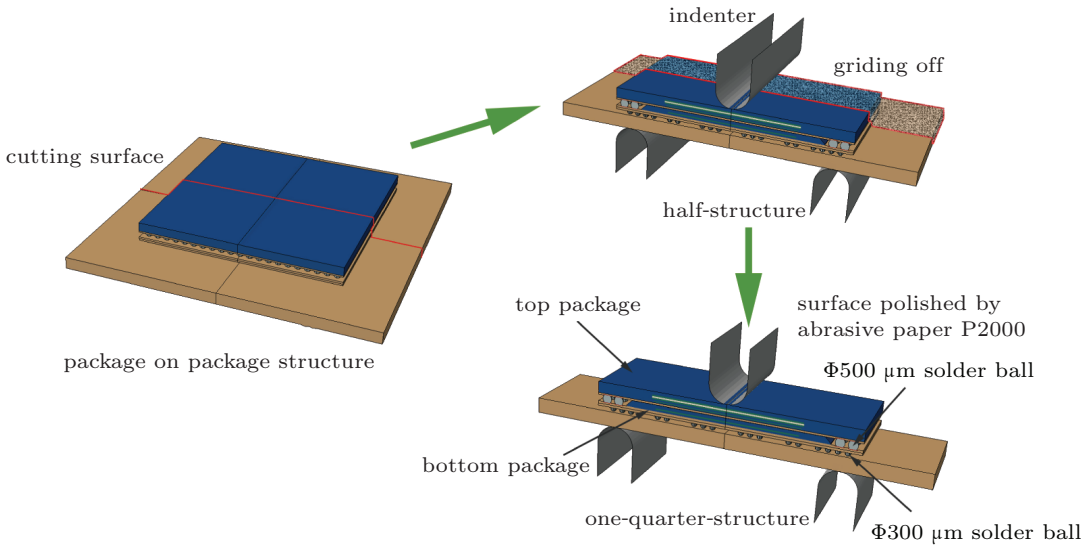


Fig. 2. (colour online) Schematic diagram of the specimen making.

2.1. Experimental procedure

Three-point bending tests are carried out by an electro-hydraulic servo testing machine (Shimadzu, Japan). The specimen is placed in the vacuum chamber (10^{-4} Pa) for observation by the SEM during the bending tests. The signal of SEM is directly transferred to a computer, making it possible to obtain 960×1280 pixels of SEM image. Displacement control loading with the loading speed 4.0×10^{-4} mm/min is used in the test, and the bending span is 10 mm. The loading history and the images of the specimen cross section are recorded respectively.

2.2. Experimental results

2.2.1. Half-structure test based on *in-situ* SEM observation

For the sample under applied bending loading, the cracks occur first in die C and then discontinuously occur in die B and die A in sequence as shown in Fig. 3(a). This is because these layers are relatively more brittle than other die attach layers. With the increase of the bending loading, multi-cracks appear in the DA and connect the isolated cracks in different dies into a continuous crack as shown in Figs. 3(b). A notable phenomenon is that the cracks are not initiated in the middle of the specimen which is generally regarded as the most frail region. However, the cracks propagate to the middle region with the increase of the bending loading as shown in Fig. 3(c). Then the cracks propagate to the substrate layer. The cracks in substrate and die C each have an obvious deflection and bridging, indicating that the crack initiation and propagation behaviour of a composite material are typical phenomena of crack deflection/branching and bridging as shown in Fig. 3(d).

2.2.2. One-quarter-structure test based on *in-situ* SEM observation

In this test, the one-quarter-structure (different from the half-structure in the restricting condition) is ground into a significant laminating structure composed of dies, die attach, and substrate. The stiffness decreases dramatically and results in the carrying capacity of the structure decreasing. The *in-situ* SEM observation of the cross section is shown in Fig. 4(a).

The crack initiation sequence is similar to that in the half-structure test: die C, die B, die A, and die attach. The cracks in die C and die B occur in pairs almost symmetrically to the symmetry axis of the structure as shown in Fig. 4(b). With the increase of the applied loading, another crack occurs approximately in the symmetry axis as shown in Fig. 4(c). Then cracks in different layers are defected from their sites and bridged together and the cracks' defection widely exist in this situation due to the effect of the die attach layer as shown in Fig. 4(d). Finally, the cracks propagate to the substrate and form a long crack as shown in Fig. 4(e) and then induce the fracture of the bottom package as shown in Fig. 4(f).

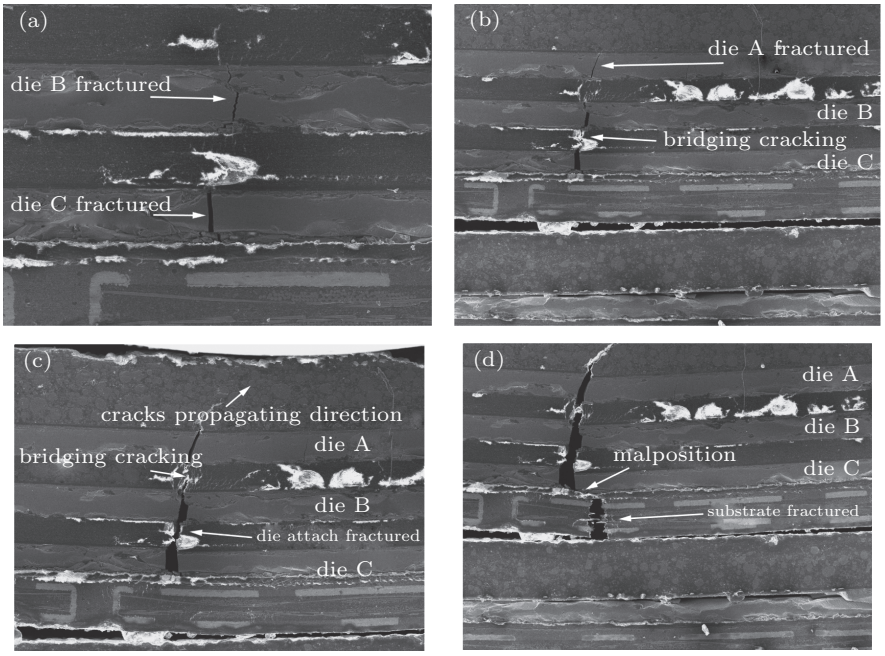


Fig. 3. *In-situ* SEM observations on cracking behaviour of half-structure under three-point-bending test. (a) Die B and die C fractured. (b) Bridging cracking of cracks in die B and die C, and die A fractured partially. (c) Bridging cracking of cracks in die A and die B, and the cracks propagate to the middle of the beam. (d) Substrate fractured and the malposition between die C and substrate.

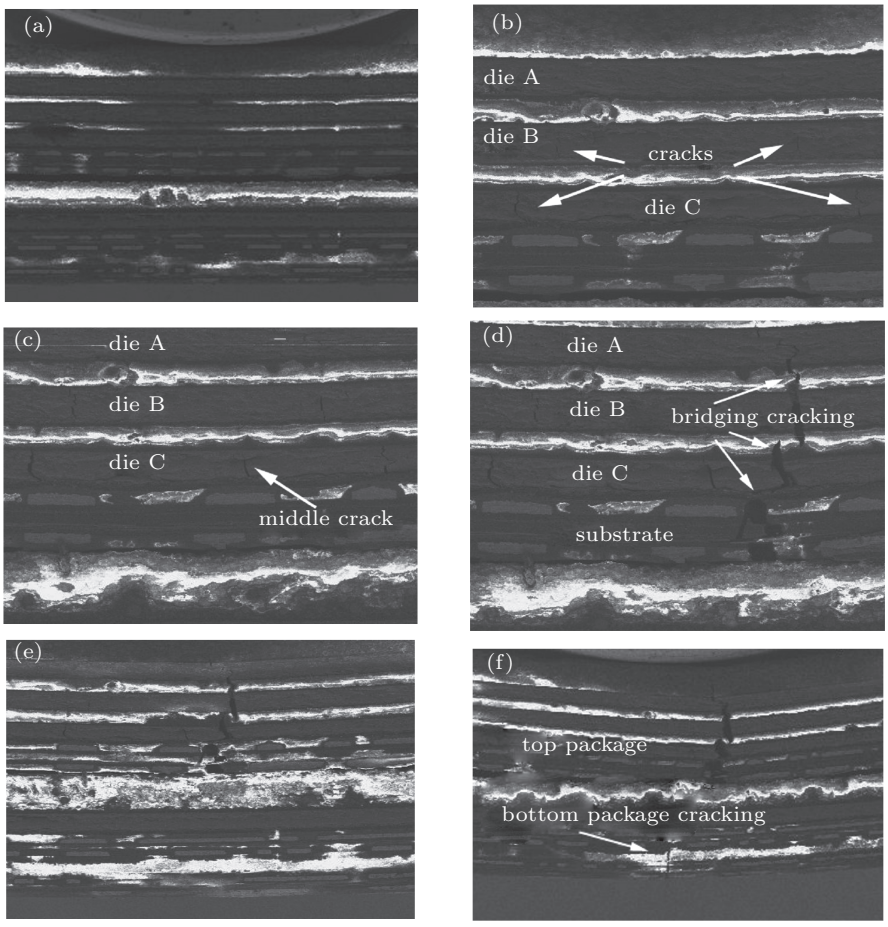


Fig. 4. *In-situ* SEM observations on cracking behavior of one-quarter-structure under three-point-bending test. (a) SEM image of the cross section. (b) Cracks in die C and die B occur in pairs. (c) Another crack in the middle of die C occurs. (d) Bridging cracking and malposition among different layers. (e) The substrate of the top package fractured. (f) The bottom package fractured.

3. Theoretical analysis

3.1. Hypotheses and simplifications

Some hypotheses and simplifications are made in favour of the analysis.

i) Because the stiffness of the dies is small compared with the whole structure, the one-quarter-structure can be regarded as a sandwich beam consisting of 8 layers with different materials and thickness, and each layer is supposed to be throughout the whole structure with no difference in length and width as shown in Fig. 5.

ii) Plane assumption exists on this occasion. The cross section is still defined as a plane vertical to the axis after deformation under applied bending loading and rotates around a certain axis vertical to the longitudinal symmetry.

iii) The failure criterion is simplified to analyse the failure process of each layer. When the maximum stress of each layer reaches the damage stress, it will be regarded as being failed.

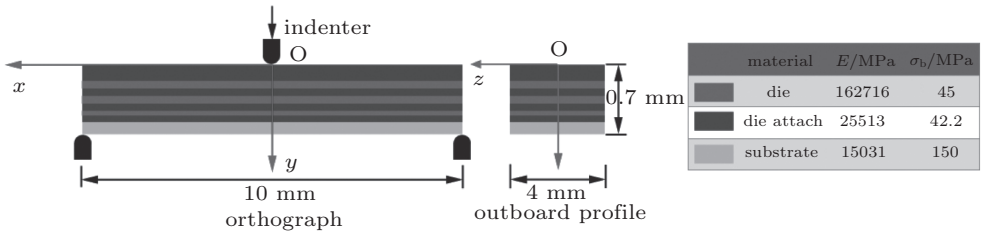


Fig. 5. Multi-layer laminating hypothesis.

3.2. Analysis procedure

The failure process of the structure is analysed in the following procedure. The first step is to input the geometric and mechanical parameters of the package structure from the data, and calculate the overall stiffness of the structure according to the material mechanics formula. The second step is to calculate the stress distribution of the mid cross section of each layer. The last step is to compare the stress levels with the damage criterion to indicate the failure extent of each layer. The stiffness values of the failed layers will be deducted from the structure, which means they only function in geometry instead of mechanics. The overall stiffness is calculated again and updated. Then the loading increases a small amount, and the new distribution of the stress is calculated. Repeat the former procedures until the failure of the whole structure appears, and the failure process of the structure can be simulated approximately.

3.3. Multi-layer laminating analysis

According to plane assumption[24] as shown in Fig. 6(a), after deformation, the axial lines ab and AB become arc-curves and vertical lines mM and nN are still straight lines. A micro unit is cut from the beam as shown in Fig. 6(b). There is no deformation in the neutral surface, and according to geometrical relationship: $\rho \mathrm{d}\theta = \mathrm{d}x$, the longitudinal strain of $\overset{\frown}{AB}$ can be written as

$$\varepsilon(y) = \frac{AB - AB_1}{AB_1} = \frac{BB_1}{O_1O_2} = \frac{y\mathrm{d}\theta}{\mathrm{d}x} = \frac{y}{\rho}, \quad (1)$$

where ρ is the radius of the axis of the structure and $\mathrm{d}\theta$ is the angle of the bending as shown in Fig. 6(b).

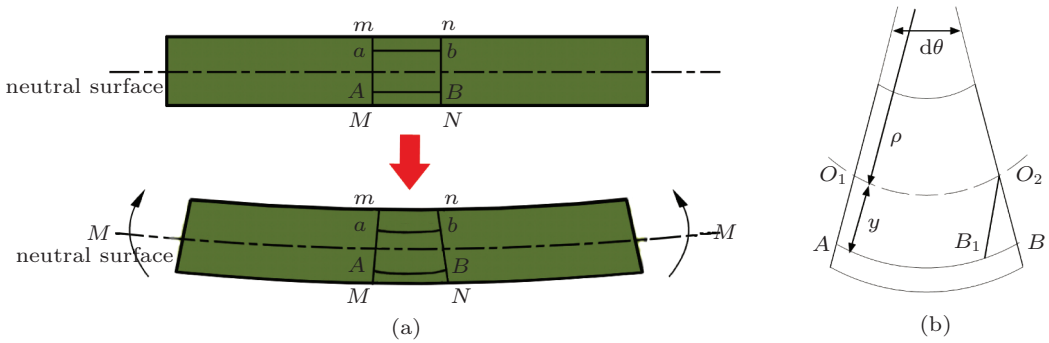


Fig. 6. (colour online) Plane assumption. (a) The deformation of beam under bending moment. (b) The deformation of a micro segment under bending moment.

The coordinate system (x, y, z) is founded as shown in Fig. 5. Then cut the beam into two equal-size parts in the mid cross section (plane yOz) to analyse the stress distribution in the cross section as shown in Fig. 7.

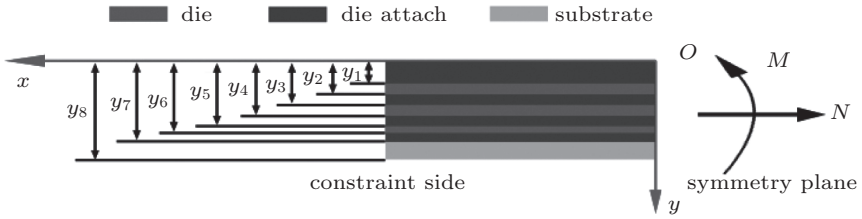


Fig. 7. Force analysis of the mid cross section.

According to Hooke's law, the constitutive equations can be simply written as

$$\sigma(y) = E(y)\varepsilon(y), \tag{2}$$

where E is the Young's modulus of elasticity of each layer of the beam. Both E and ε are the functions of ordinate y.

The equilibrium equations can be written as

$$\begin{aligned} M &= \int_A \sigma(y)(y - y_{\rm na})\,{\rm d}A \\ &= \int_\Gamma B\sigma(y)(y - y_{\rm na})\,{\rm d}\Gamma, \end{aligned} \tag{3}$$

$$N = \int_A \sigma(y)\,{\rm d}A = \int_\Gamma B\sigma(y)\,{\rm d}\Gamma, \tag{4}$$

where M and N are the bending moment and axial force applied to the beam at $x = 0$ (mid cross section of the beam), $\sigma(y)$ is the normal stress of the cross section at each point, $y_{\rm na}$ is the ordinate of the neutral axis, A and Γ are the surface zones of the cross section in three-dimensional (3D) and two-dimensional (2D) formation. B is the breadth of the beam in the z direction.

Considering geometric equation (1) and constitutive equation (2), equations (3) and (4) can be rewritten as

$$\begin{aligned} M &= \int_\Gamma BE(y)\frac{(y - y_{\rm na})^2}{\rho}\,{\rm d}y \\ &= \int_{\Gamma_1} BE_1\frac{(y - y_{\rm na})^2}{\rho}\,{\rm d}y \\ &\quad + \int_{\Gamma_2} BE_2\frac{(y - y_{\rm na})^2}{\rho}\,{\rm d}y + \cdots \\ &\quad + \int_{\Gamma_n} BE_n\frac{(y - y_{\rm na})^2}{\rho}\,{\rm d}y \\ &= \frac{B}{\rho}\sum_{i=1}^{n}\int_{y_{i-1}}^{y_i} E_i(y - y_{\rm na})^2\,{\rm d}y, \end{aligned} \tag{5}$$

$$\begin{aligned} N &= \int_\Gamma BE(y)\frac{y - y_{\rm na}}{\rho}\,{\rm d}y \\ &= \int_{\Gamma_1} BE_1\frac{y - y_{\rm na}}{\rho}\,{\rm d}y + \int_{\Gamma_2} BE_2\frac{y - y_{\rm na}}{\rho}\,{\rm d}y + \cdots \\ &\quad + \int_{\Gamma_n} BE_n\frac{y - y_{\rm na}}{\rho}\,{\rm d}y \\ &= \frac{B}{\rho}\sum_{i=1}^{n} E_i(y - y_{\rm na})\,{\rm d}y, \end{aligned} \tag{6}$$

where n is the number of the layers.

The above equations can be abbreviated as follows:

$$M = \frac{B}{\rho}EJ, \tag{7}$$

$$N = \frac{B}{\rho}S^*_{\rm na}, \tag{8}$$

where

$$EJ = \sum_{i=1}^{n}\int_{y_{i-1}}^{y_i} E_i(y - y_{\rm na})^2\,{\rm d}y \tag{9}$$

is the moment of inertia with respect to the neutral axis ($y = y_{\rm na}$) of the cross section representing the flexural stiffness of the beam, and

$$S^*_{\rm na} = \sum_{i=1}^{n} E_i(y - y_{\rm na})\,{\rm d}y \tag{10}$$

is the static moment of the cross section with respect to the neutral axis ($y = y_{\rm na}$) of the cross section.

In the three-point-bending test, M can be calculated by the applied load and N can be regarded as 0, respectively. So EJ and $y_{\rm na}$ can be obtained through solving Eqs. (7)–(10).

According to flexure formula, the stress distribution of the cross section can be written as follows:

$$\sigma(y) = \frac{M}{EJ}E(y)(y - y_{\rm na}), \tag{11}$$

where M is the bending moment, EJ is the moment of inertia with respect to the neutral axis as indicated in Eq. (9), and E is the Young's modulus of elasticity and a piecewise function in this situation, specially.

3.4. Results

The failure processes and the stress distributions are calculated by Eq. (11) through applied monotonous deflection bending loading from 0 mm to 1.7624×10^{-1} mm respectively as shown in Figs. 8(a)–8(h). The bending moment is used to represent the loading level during the analysis. When the bending moment reaches 5.6851 N·mm, the maximum stress of die C is 45 MPa, indicating that die C fails according to the simplified failure criterion as shown in Fig. 8(a) and when the bending moment reaches 7.1117 N·mm, die B fails as shown in Fig. 8(b). With the increase of the loading level, the DA (between the substrate and die C) fails with the maximum stress reaching 42.2 MPa as shown in Fig. 8(c). Then the DAs (between die B and die C) and die A fail successively with the bending moment reaching 12.9207 N·mm and 14.3367 N·mm as shown in Figs. 8(d)–8(e), respectively. Three dies fail completely at this loading level. When the bending moments reach 26.6274 N·mm and 31.1948 N·mm, the DA (between die A and die B) and the substrate fails as shown in Figs. 8(f) and 8(g), respectively. Finally, the last DA (above die A) fails when stress reaches a maximum value of 42.2MPa, and the loading level reduces to 1.0489 N·mm due to the reduction of the stiffness as shown in Fig. 8(h). The theoretical analyses of the failure processes are consistent with the experimental results based on *in-situ* SEM observations as shown in Figs. 3 and 4.

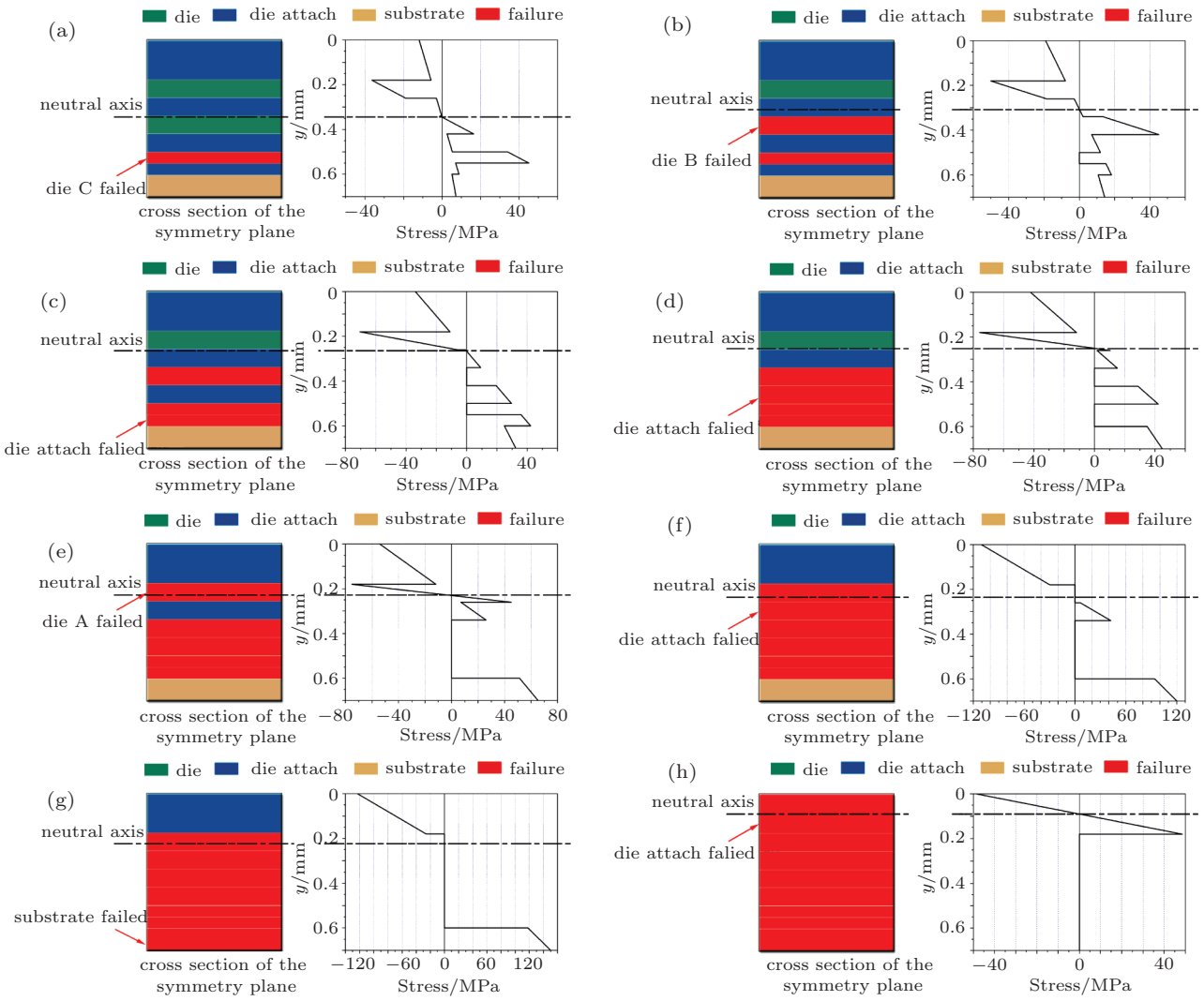


Fig. 8. (colour online) Failure processes and stress distributions of the structure under different values of loading M : M = 5.6851 (a), 7.1117 (b), 12.2353 (c), 12.9207 (d), 14.3367 (e), 26.6274 (f), 31.1948 (g), and 1.0489 N·mm (h).

3.5. Discordance analysis

The theoretical analysis indicates that the cracks occur in the middle of the beam under three-point-bending where the biggest normal stress is generated. However, the one-quarter structure test shows that the cracks occur in a nearby region and come into being in pairs, mostly.

Practically, the one-quarter structure has a low stiffness and as a result the beam can deform easily. Once the indenter presses on the beam, the force is more like a uniform pressing than a concentration force; and the structure is of small size, the uniform press region is comparable to the length of the beam, which will affect the bending moment distribution distinctly as shown in Fig. 9. Another factor that will affect the cracking is the surface strength, which can be easily influenced by polish. So the cracks occur in the cracking region randomly, and the cracking region is smaller in the inner places because of the stress gradient in the cross section.

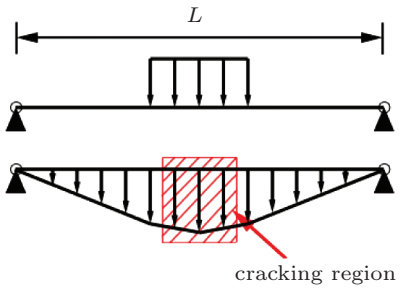


Fig. 9. (colour online) Real bending moment distribution and cracking region.

4. Conclusions

In-situ SEM observation method is used to investigate the failure process of the PoP structure under three-point bending loading and mechanics principles are used to analyse the failure sequence of each layer in the top package based on the multi-layer laminating hypothesis and plane assumption. The conclusions are drawn as follows.

(I) The failure of the PoP structure under three-point-bending loading has a significant layer failure phenomenon and the discontinuous crack initiation behaviour and the crack defecting and bridging propagation behaviour are affected by the DA plastic layer.

(II) Multi-layer laminating hypothesis and plane assumption can be used approximately to estimate the failure of the PoP structure under bending loading and to illuminate the failure of each layer exactly.

(III) *In-situ* SEM observation technology can play an important role in investigating the failure process of structures in micro-scale such as the PoP structure.

References

[1] Yoshida A, Taniguchi J, Murata K, Kada M, Yamamoto Y, Takagi Y, Notomi T and Fujita A 2006 *Proceedings of the* 56*th Electronic Components and Technology Conference* (San Diego: Institute of Electrical and Electronics Engineers)

[2] Dreiza M, Yoshida A, Ishibashi K and Maeda T 2007 *Proceedings of the* 57*th Electronic Components and Technology Conference* (Reno: Institute of Electrical and Electronics Engineers)

[3] Tian M B 2003 *Electronic Packaging Technology* (Beijing: Tsinghua University Press) p. 20 (in Chinese)

[4] Sawada Y, Yamaguchi A, Oka S and Fujioka H 1998 *IEMT/IMC Symposium* (Tokyo: IEEE CPMT Society)

[5] Lin J C, Yu J, Chung B, Chang K and Fang D 2011 *Proceedings of the* 61*st Electronic Components and Technology Conference* (Lake Buena Vista: Institute of Electrical and Electronics Engineers)

[6] Sommer J P, Michel B, Hofmann T, Gottwald T, Neumann A and Podlasly A 2011 *Electronic Packaging Technology & High Density Packaging* (Shanghai: Electronic Manufacturing and Packaging Technology Society)

[7] *International Technology Roadmap for Semiconductors (ITRS) — Assembly and Packaging* 2007 available: http://www.itrs.net/Links/2007ITRS/Home2007.htm

[8] Winkler S 2007 *Advanced IC Packaging* (Electronic Trend Publications Inc.)

[9] Lee J Y, Hwang T K, Kim J Y, Yoo M, Sohn E S, Chung J Y and Dreiza M 2007 *Proceedings of the* 57*th Electronic Components and Technology Conference* (Reno: Institute of Electrical and Electronics Engineers)

[10] Zhang G C, Feng S W, Zhou Z, Li J W and Guo C S 2011 *Chin. Phys.* B **20** 027202

[11] Sun P, Leung V C, Xie B, Ma V W and Shi D X 2008 *Electronic Packaging Technology & High Density Packaging* (Shanghai: Electronic Manufacturing and Packaging Technology Society)

[12] Wang X S, Li Y and Meng X K 2009 *Sci. Chin.* E: *Tech. Sci.* **52** 2201

[13] Amagai M, Suzuki Y, Abe K, Kim Y B and Sano H 2008 *Proceedings of the* 58*th Electronic Components and Technology Conference* (Lake Buena Vista: Institute of Electrical and Electronics Engineers)

[14] Lee S R, Lui B H W, Kong Y H, Baylon B, Leung T, Umall P and Agtarap H 2002 *Soldering & Surface Mount Tech.* **14** 46

[15] Yao B, Lai P, Liu J and Liang X S. 2011 *International Symposium on Advanced Packaging Materials* (Xiamen: IEEE's Components Packaging and Manufacturing Technology Society)

[16] Liu H L and Yang S H 2011 *International Conference on Quality, Reliability, Risk, Maintenance, and Safety Engineering* (Xi'an: Institute of Electrical and Electronics Engineers)

[17] Lau H J, Pan H S and Chang C 2001 *Int. J. Microcircuit and Electronic Packaging* **24** 1

[18] Wang X S, Li X D, Ren H H, Zhao H Y and Murai R 2011 *Microelectron. Reliab.* **51** 1377

[19] Ren H H, Wang X S, Chen Y L and Li X D 2012 *Chin. Phys.* B **21** 034501

[20] Wang X S, Xu Y and Xu Q X 2004 *Appl. Compos. Mater.* **11** 145

[21] Wang X S, Wu B S and Wang Q Y 2005 *Cement and Concrete Res.* **35** 1385

[22] Wang X S, Ji L, Li Y and Guo X W 2008 *Mater. Lett.* **62** 1856

[23] Sun P, Leung V, Yang D, Lou R, Shi D and Chung T 2010 *Proceedings of the* 60*th Electronic Components and Technology Conference* (Las Vegas: Institute of Electrical and Electronics Engineers)

[24] Fan Q S and Yin Y J 2004 *Material Mechanics* (Beijing: Tsinghua University Press) p. 90 (in Chinese)